© Universiti Tun Hussein Onn Malaysia Publisher's Office

IJIE

http://penerbit.uthm.edu.my/ojs/index.php/ijie
ISSN : 2229-838X e-ISSN : 2600-7916

The International Journal of Integrated Engineering

Characteristic of Thin Sheet Membrane for a Mechanical Driven Micropump System

MQA Rusli[1], Pei Song Chee[2], Pei Ling Leow[1*], Rashidah Arsat[1], Ruzairi Abdul Rahim[3]

[1]School of Electrical Engineering, Faculty of Engineering,
Universiti Teknologi Malaysia, Skudai, 81310, JOHOR

[2]Lee Kong Chian, Faculty of Engineering and Science,
Universiti Tunku Abdul Rahman, Kajang, 43000, SELANGOR

[3]Faculty of Electrical and Electronic Engineering,
Universiti Tun Hussein Onn, Parit Raja, 86400, JOHOR

*Corresponding Author

DOI: https://doi.org/10.30880/ijie.2019.11.01.001
Received 25 January 2018; Accepted 21 February 2019; Available online 30 April 2019

Abstract: This paper demonstrates the characteristic of a thin sheet membrane for a mechanical driven micropump system by using a spin coater technique. The moving diaphragm for the micropump system was made from a PDMS polymer material. A plastic lidded dish with a diameter of 100 mm and height of 15 mm was used as a mould for this study. There were three variables that influence the membrane thickness formation during the spin coating process, which are the polymer weight, spin speed and the spinning time. It was observed that the final parameters to fabricate a thin sheet membrane are 2.5 g of PDMS polymer weight, 500 rpm of spinning speed and 180 s of spin time to yield a 314.82 ± 3.6556 µm thin membrane. This characteristic study is foresee could serve as a design guideline to fabricate a thin sheet membrane for a mechanical driven micropump system by using a petri dish as an alternative to a silicon wafer.

Keywords: Thin sheet membrane, mechanical micropump, PDMS polymer

1. Introduction

A thin sheet membrane is considered to be the key functional component in a mechanically driven micropump system, especially in microvalve [1-6] and valveless [7, 8] micropump family. The external force acting on the membrane sheet pulls up or down the diaphragm to allow the fluid to move inside the channel. Numerous research and studies have focused on the manipulation of the channel geometry to achieve the desired flow in term of direction and flow rate [3, 9-12]. In most common reported design, the membrane is coupled to a piezoelectric disc [13, 14], a magnetically driven actuator [15] and a DC micromotor actuator [16, 17]. In particular, polydimethylsiloxane (PDMS) material is widely used in the fabrication and prototyping of the micropump design because of the rapid fabrication, reasonable cost and ease of implementation [13, 18, 19].

This work describes a characteristic of a thin sheet membrane prepared from PDMS polymer material as a flexible diaphragm for the mechanically driven micropump system. The PDMS polymer comes in the combination of the monomer resin (base) and the curing agent (hardener), changing the liquid state (pre-polymer) to the solid state (polymer). The monomer resin is much more viscous than the curing agent. PDMS microstructure components are most

*Corresponding author: leowpl@utm.my

frequently fabricated with thicknesses greater than 200 µm and using the manufacturers recommended mix ratio of 10:1 (w:w) because the cross-linked in the polymer are well defined [20]. To produce a uniform flat membrane, a spin coater machine was used to spread the pre-polymer material over a petri dish as the mold for the membrane sheet fabrication. This method was used to enable the rapid fabrication features, especially during a batch making of the membrane sheet. The flexible membrane utilizes an asymmetrical vibration profile to induce a pressure gradient that rectifies the fluid flow and thus generates a net pumping effect. This mechanism was further clarified by experimental studies to the membrane displacement during actuation conditions with a complete setup of an electromagnetic actuated micropump system.

2. Working Principle of Membrane Sheet

The fluid flow inside the micropump is produced from the stroke capability of the oscillating diaphragm from the working membrane. The operation of the membrane with an electromagnetic actuated micropump with Neodymium Iron Boron (NdFeB) magnet is illustrated in Fig. 1.

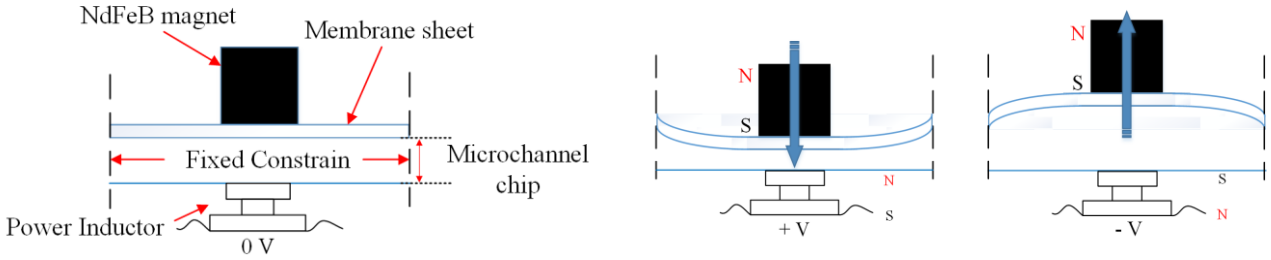

(a) (b) (c)

Fig. 1 The operation of NdFeB permanent magnet acting on a thin sheet membrane (a) steady-state condition (b) attractive condition (c) repulsive condition

Fig. 1 shows the operation of the NdFeB permanent magnet acting on a thin sheet membrane during initial and electromagnetic force induced state. The membrane edges are set to a fixed constraint mode in order to achieve a deflection profile of the membrane. The permanent magnet adheres at the top center of the membrane and the power inductor is placed at the bottom aligned with the permanent magnet. The oscillation of the NdFeB magnet is influenced by the polarity of the supplied voltage from the power inductor to attract and repel the magnet [1, 2]. During the initial state (Fig. 1 (a there is no voltage is induced. When a positive polarity voltage is induced to the power inductor as shown in Fig. 1 (the membrane displacement was observed in a downward direction. The membrane is deflected to expel the working fluid through the channel. On the other hand, a negative polarity voltage is applied, the membrane is observed deflected in an upward direction and thus, the fluid enters into the chamber (Fig. 1 (c)). The continuous cycle of the voltage polarities to attract and repel the magnet create a net fluid flow inside the microchannel. Different cycle speed (actuation frequency) induced from the actuator module gives a different flow rate to the micropump system [1, 3]. For example, the electromagnetic actuated micropump developed by Shen M. *et al.* capable to produce variation of flow rates by inducing a different frequency setting from the rotating motor such as 12 Hz and 15 Hz of the actuation frequencies producing 2.4 mL/min and 2.4 mL/min of flow rate, respectively [1].

3. Membrane Material Properties Study

Two different membrane properties were selected based on the commonly used by the previously reported research; silicon and PDMS polymers [4-6]. For this work, the suitable membrane material is selected based on its ability to elongate without breaking it under a given force. The numerical technique was conducted by using COMSOL Multiphysics® software (COMSOL Inc., Burlington, USA) to perform the finite element analysis (FEA). The density, Young's modulus and Poisson's ratio of the Si material are 2320 kgm^{-3}, 130.2 GPa and 0.28, respectively [7], meanwhile for the PDMS material are 965 kgm^{-3}, 1.32 MPa and 0.499, respectively [5, 6]. Both properties value are based on its curing temperature; different curing temperature gives different Young's modulus value [6]. To evaluate the performance comparison on both materials, a thin sheet membrane coupled with a NdFeB permanent magnet was designed and the geometry design is illustrated in Fig. 2.

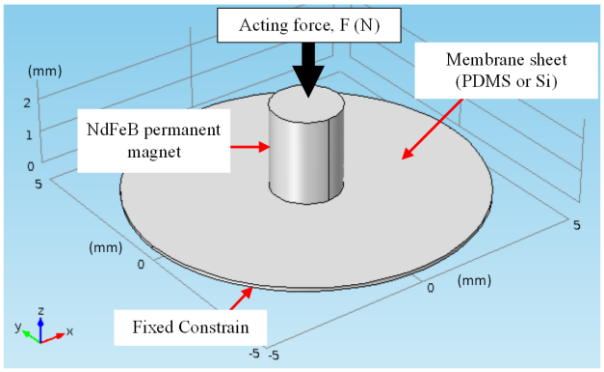

Fig. 2 Geometry design for membrane properties study

Fig. 2 shows the geometry design to investigate the membrane displacement and stress on both selected materials. The performance on both materials is studied using the numerical model where the thin sheet membrane is coupled with a cylindrical NdFeB magnet. In order to deflect the membrane sheet, the surface contact ratio between the permanent magnet and the membrane sheet should be less than 1. For this study, the surface contact ratio between the magnet and thin sheet membrane is set to 0.4 [8]. The membrane edges are set to a fixed constraint mode so that the membrane sheet able to deflect when a force is applied. The acting force was applied on the magnet from 0.1 N to 1 N in a –z-direction (downward). The finite element analysis result in both Si and PDMS material is shown in Fig. 3.

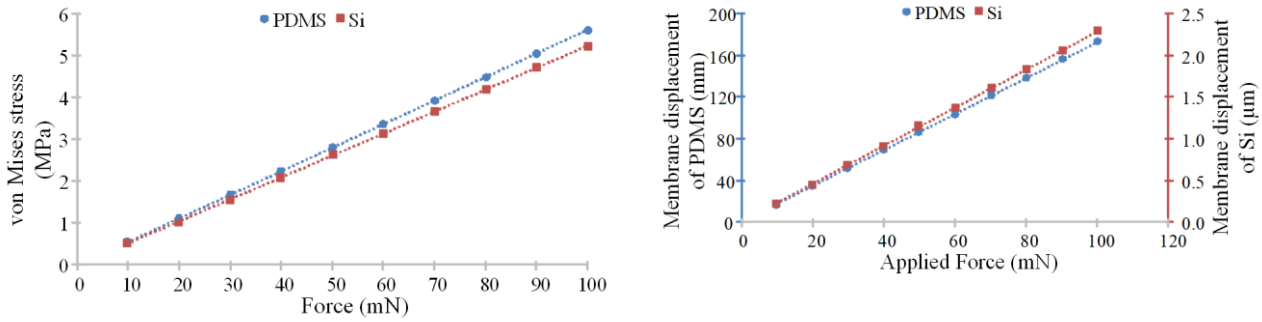

(a) (b)

Fig. 3 Stress and displacement plot of PDMS and Si (a) von Mises stress vs. applied force (b) membrane displacement vs. applied force

Fig. 3 shows the finite element analysis result on both materials between the membrane stress and displacement based on the applied force respectively. Both readings are taken at the center of the thin sheet membrane. As shown in Fig. 3 (a), at the maximum applied force, which is on 100 mN, the stress difference between the PDMS and Si materials only exist at a small difference by 6.79 % of von Mises stress. In contrast, the membrane displacement results from Fig. 3 (b) shows that at the maximum applied force, the displacement of the PDMS material is greater than Si material by the difference of 98.67 %.

Thus, based on this study, the PDMS material is more elastic than Si material because the value of Young's modulus of the PDMS material is lower than Si material. Therefore, the ability of the Si material to withstand changes (stiffness of material) in length under a lengthwise tension is longer than PDMS material, even though the stress on both materials only shows a small difference. Hence, PDMS material is selected for this work to fabricate a thin sheet membrane for the flexible diaphragm to the micropump system.

4. Development of Thin Sheet Membrane

The membrane material is selected based on its ability to elongate under a given force without breaking itself. The flexible thin sheet membrane was fabricated by using a polydimethylsiloxane (PDMS) polymer from SYLGARD® 184 Silicone Elastomer Kit (Dow Corning Corporation, USA) with a mixing ratio of the resin to hardener 10:1 (w/w). Petri dish (Fisher Scientific, Pittsburgh, USA) with a diameter of 100 mm and a height of 15 mm was used as a mold for the membrane. The use of a petri dish instead of a disc plate that generally have been used by many researchers in the making of membrane sheet is to avoid the excessive PDMS polymer being thrown away during the spinning process. The usage of petri dish can avoid polymer wastage and contamination to the spin coater machine. During the spinning process, the solution can spread evenly in all areas but remain in the petri dish. A digital spin coater machine with a spinner (TJ9000, Torch Inc, Beijing, China) was used to yield a uniform pre-polymer for the membrane in a sheet shape. Meanwhile, the membrane was measured by using a precision digital micrometer (5202-52, Sanhe Ltd,

Zhejiang, China). The main challenge of the fabrication was to produce a thin sheet flat surface membrane since the thin PDMS membrane easily to break when it is peeled out from the mold. The process of membrane coating as illustrated in Fig. 4.

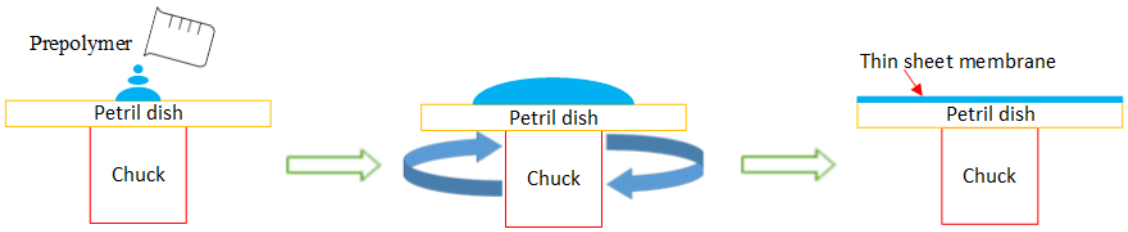

Fig. 4 The process of thin PDMS membrane coating (a) pre-polymer dispersing (b) spreading (c) coating

Fig. 4 shows the procedure for the membrane coating by using a spin coater machine. The measured PDMS pre-polymer was poured in the center of the plastic petri dish. Then, it was placed in the spin coater machine for spinning process. After that, it was placed in an oven for the curing process. The spin-coated polymer was then cured in an oven at 70 °C for 30 minutes [6]. The thickness of the membrane was measured with a digital micrometer. Fig. 5 shows the measurement points to evaluate the cured membrane on the dish. The average and standard deviation for the membrane thickness were then calculated. Finally, the membrane was slowly peeled off from the petri dish.

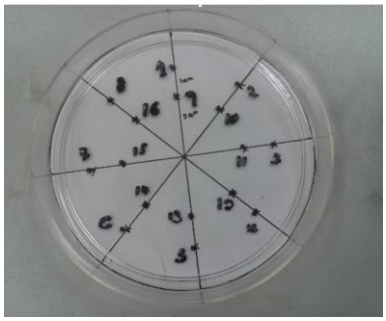

Fig. 5 Sixteen points of measurement to measure the membrane thickness

In theory, the calculation for an ideal membrane thickness as follows:

Volume of cylindrical (petri dish),

$$v = \pi r^2 t_m \text{, m}^3 \quad (1)$$

Density of PDMS polymer,

$$\rho = \frac{m}{v} \text{, kgm}^3 \quad (2)$$

Therefore, the equation (1) into the equation (2),

$$t_m = \frac{m}{\rho \pi r^2} \text{, m} \quad (3)$$

Where,
r is the radius of thin sheet membrane in m,
t_m is the membrane thickness in m,
m is the polymer weight in kg.

The density of PDMS polymer under the atmospheric condition is 965 kgm^{-3}, therefore, from the equation (3), the yield output thickness is 329.855 µm from 2.5 g of the dispensed PDMS polymer.

There are three variables that influence the membrane thickness formation during the spin coating process, which are the polymer weight, spin speed and the spinning time. Therefore, in the following Section 4.1 to Section 4.3, we have investigated to select the suitable parameter to fabricate the thin sheet membrane based on these three parameters.

4.1 Membrane Thickness Influenced by a PDMS Polymer Weight

This experimental study was to investigate the influence of the dispensed PDMS polymer to the membrane thickness during the spinning process. The PDMS polymer weight is varying from 2 g to 7 g. The spin speed and spin time are 500 rpm and 120 s respectively. The fabrication result is plotted as shown in Fig. 6.

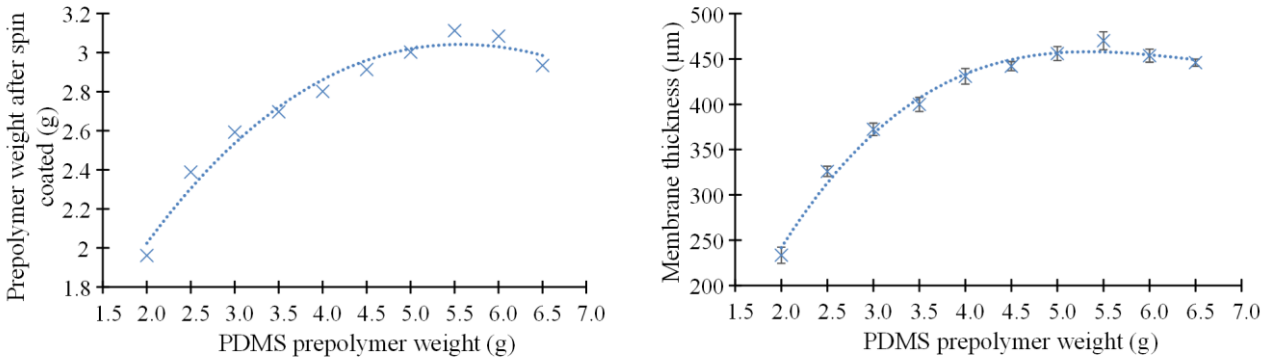

(a) (b)

Fig. 6 Fabricated membrane over a variation of PDMS polymer weight (a) PDMS polymer weight after the spin-coated (b) the cured membrane thickness

From Fig. 6, the membrane thickness increases as the PDMS weight increases from 2 g to 5.5 g. When the weight is over 5.5 g, the membrane thickness starts to decrease. This is due to the excessive weight placement inside the petri dish; the pre-polymer material starts to splatter away from the dish during the spinning process. However, as the weight of 2 g of PDMS, the mixture was not fully spread over the dish with some part of the cured PDMS pre-polymer in the petri dish easily torn out during the peeling process. The surface conditions of the PDMS pre-polymer spread across the petri dish are shown in Fig. 7.

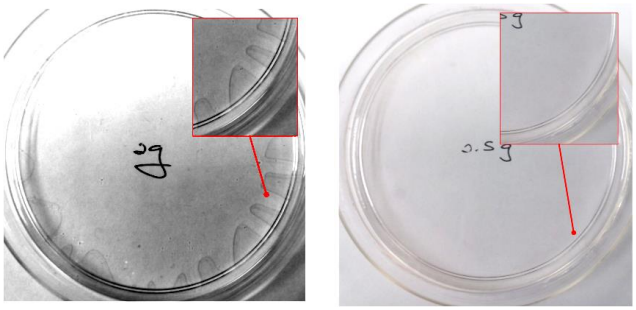

Fig. 7 A side-by-side comparison between even and uneven spread after spin coated (a) 2 g of PDMS solution (uneven spread) (b) 2.5 g of PDMS solution (even spread)

Fig. 7 shows the spin-coated 2 g and 2.5 g of PDMS pre-polymer inside the petri dish. The 2 g of PDMS pre-polymer has an uneven spread over the petri dish because the pre-polymer quantity is not enough to spread the entire dish during the spinning process. As the weight of pre-polymer increases, the thickness increases that subsequently causes the elasticity of the membrane to reduce. As the membrane elasticity decreases, the actuation module requires more force to attract and repel the membrane.

From this experiment, 2.5 g is the starting weight to produce an even spread membrane inside the petri dish with spin speed and time taken of 500 rpm and 120 s respectively, yield 325.90 ± 5.685 µm of thickness.

4.2 Membrane Thickness Influenced by Spin Coater Speed

This study was conducted to investigate the spin coater machine's speed in order to produce an even thin sheet membrane by using a PDMS pre-polymer. The experiment was conducted by fixing the value of pre-polymer weight at 2.5 g and spin time at 120 s, but vary the spin coater machine's speed from 200 rpm to 700 rpm. The experimental results are shown in Fig. 8.

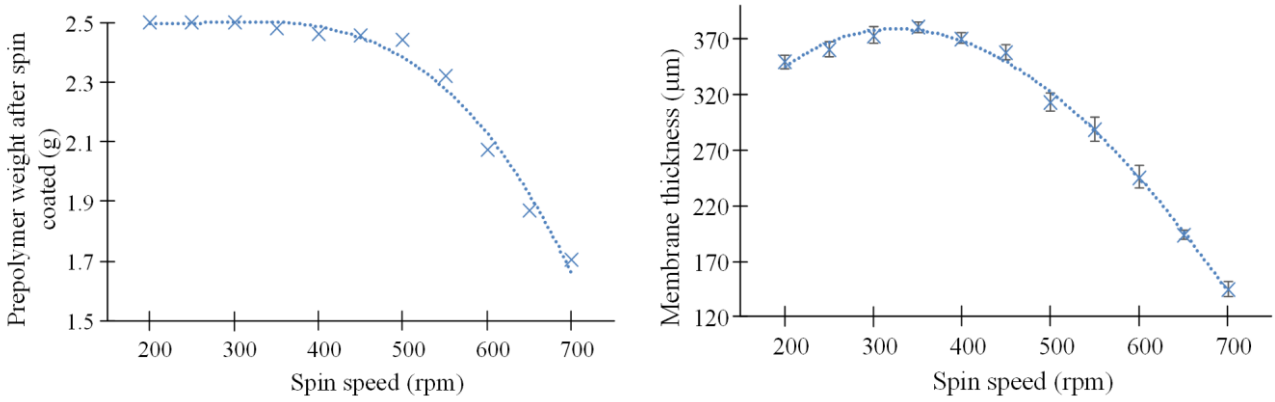

(a) (b)

Fig. 8 Fabricated membrane over the variation of spin coater speed setting (a) polymer weight after spin coated (b) membrane thickness

Fig. 8 shows the weight and membrane thickness profile with respect to the spinning rate (rpm) of the spin coater machine. It was observed from 200 rpm to 300 rpm of spinning rate, the PDMS pre-polymer was unable to cover completely the whole area inside the dish. This is because the spinning speed was slow and the centrifugal force was not sufficient to spread the pre-polymer completely in all areas inside the petri dish for the given time. However, from 350 rpm to 700 rpm, the pre-polymer spread equally in all areas. From the observation, at a spin rate 550 rpm to 700 rpm, the membrane was easily torn during the peeling process.

This experiment shows that the spinning rate at 500 rpm is suitable for 2.5 g of PDMS pre-polymer at 120 s of time taken to produce the membrane thickness of 313.67 µm.

4.3 Membrane Thickness Influenced by Spin Time

This experiment studies the spinning time required for spreading 2.5g of pre-polymer with a constant spin speed at 500 rpm. Ten sets of 2.5 g of pre-polymer were spun for various length of time at the same spin speed and the final cured membrane thickness are recorded and plotted as shown in Fig. 9.

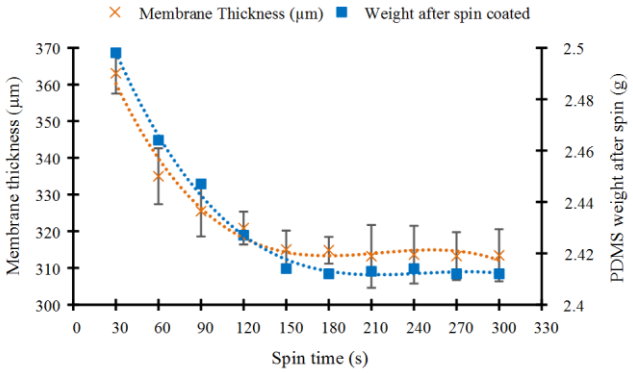

Fig. 9 Membrane thickness over spin time

From Fig. 9, the thickness and the weight of the membrane are stabilized after spinning for 150 s. Onwards, the membrane starts to maintain its thickness between 314 µm to 315 µm after 150 s. From the observation, the pre-polymer is able to cover the whole area of the dish after 90 s of spinning time. Furthermore, pre-polymer that spins for 180 s up to 300 s produces uniform and thin membrane sheet, which is easily peeled off from the petri dish without breaking the membrane structure.

In summary, from these three studies on Section 4.1 to Section 4.3, three experiments were conducted on polymer (PDMS) thickness-dependent relationships in term of pre-polymer weight, spin speed and spin time. It was observed that the final parameters to fabricate a thin sheet membrane for this work are 2.5 g of PDMS solution weight, 500 rpm of spinning speed and 180 s of spin time to yield a 314.82 ± 3.6556 µm thin membrane.

5. Membrane Displacement Study

Performance of the fabricated membrane from Section 4.2 is tested by integrating the membrane to the electromagnetic actuator micropump system. The diameter of the pumping chamber is 10 mm and the surface contact

ratio between the NdFeB permanent magnet to the chamber is 0.4. Experimental setup for the membrane evaluation is shown in Fig. 10.

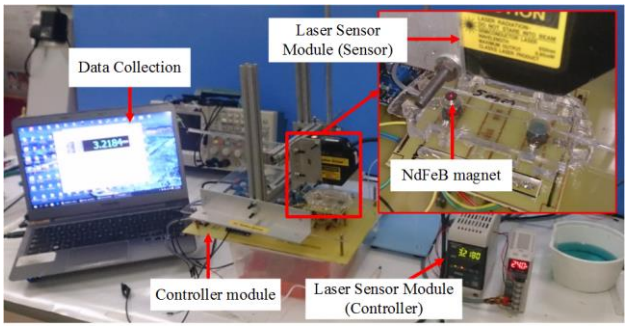

Fig. 10 Experimental setup for membrane displacement with a laser sensor module.

Fig. 10 shows the experimental setup to measure the membrane displacement in attract and repel condition. The membrane displacement was measured by using a digital CMOS laser sensor module (LK-G32, KEYENCE Corp., Japan). The laser sensor was positioned over the top center of the permanent magnet. LK-Navigator software interface (KEYENCE Corp., Japan) was used for data collections. The measurement operation is schematically illustrated in Fig. 11.

(a) (b)

Fig. 11 Membrane displacement measurement operation at (a) attractive condition (b) repulsive condition

Fig. 11 shows the membrane displacement at attractive and repulsive conditions due to the changes of the voltage polarity of the power inductor device. According to the datasheet (Coilcraft Inc., D03308P), the permissible maximum voltage can be supplied to the power inductor is 1.4 V_{dc}. However, the maximum tested supply was set up to 1.5 V_{dc} in order to investigate the effect of membrane displacement when the power inductor is oversupply.

The direction of the magnetic field depends on the induced current to the winding coil, which is producing a North and South polarities at both ends of the core. The magnet or ferromagnetic material placed near the power inductor causes the attractive or repulsive force when the power inductor is magnetized. The electromagnetic force is denoted in Equation (4).

$$F = \frac{(N \times I)^2 \times \mu_0 \times A}{2 \times (t_{Mi})^2}, \text{N} \qquad (4)$$

Where;
F is the electromagnetic force in N,
N is the number of turns (turns),
I is the induced current in A,
μ_o is the permeability of free space ($4\pi \times 10^{-7}$ H/m),
A is the area of cross section of ferromagnetic material in m^2,
t_{Mi} is the length of the gap between the power inductor and the magnet in m.

Based on Equation (4), the three elements that influence the formation of electromagnetic force strength are the number of turns, current value and the length of the gap between the solenoid and a piece of metal. The input current direction and a coil winding (clockwise or anti-clockwise) influence the attractive and repulsive direction of the disc plate. Within the coils, a strong magnetic field arises whenever current flows through the wire.

Three studies were conducted to investigate the membrane displacement based on various magnet diameters, the distance between the magnet and power inductor, and the medium inside the chamber.

5.1 Magnet Diameter

This experiment was conducted by using a 5 mm of channel module with three different magnets of 4 mm, 5 mm and 6 mm in diameter. The supply voltage to the power inductor is range from 1.1 V to 1.5 V and the result is shown in Fig. 12.

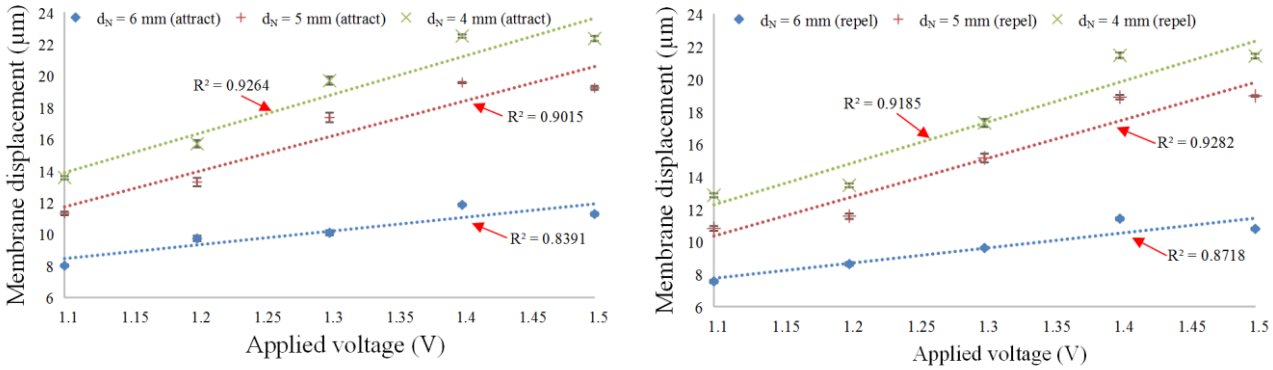

(a) (b)

Fig. 12 Membrane displacement over magnet diameter (a) attractive condition (b) repulsive condition

Fig. 12 shows the membrane displacement for the three different magnet diameter, d_N, in attractive and repulsive condition. In both conditions, when the supply voltage increases, the membrane displacement increases. However, when the voltage is exceeded to the maximum permissible voltage of the power inductor, the membrane displacement reduces slightly. For the experiment, the magnet with 4 mm diameter gives a higher displacement as compared to 5 mm and 6 mm diameter magnet.

According to the electromagnetic force theory from the equation (4), as the surface area of the permanent magnet increases, the attractive force acting from the power inductor increases as well. From Fig. 12, the magnet with 4 mm diameter gives the highest displacement as compared to 5 mm and 6 mm diameter magnet, which is contrary with the equation (4). This is due to the effect of the surface contact ratio, where the maximum membrane displacement only occurs at the 0.4 of CRs [8]. When the magnet diameter is increased over 4 mm, the membrane displacement is decreasing.

5.2 The distance between Magnet and Power Inductor

This experiment was conducted to study the membrane displacement based on the various gap between the permanent magnet and power inductor device. The studied gaps were 5 mm and 10 mm and a 4 mm of the magnet diameter was used. The experimental result is shown in Fig. 13.

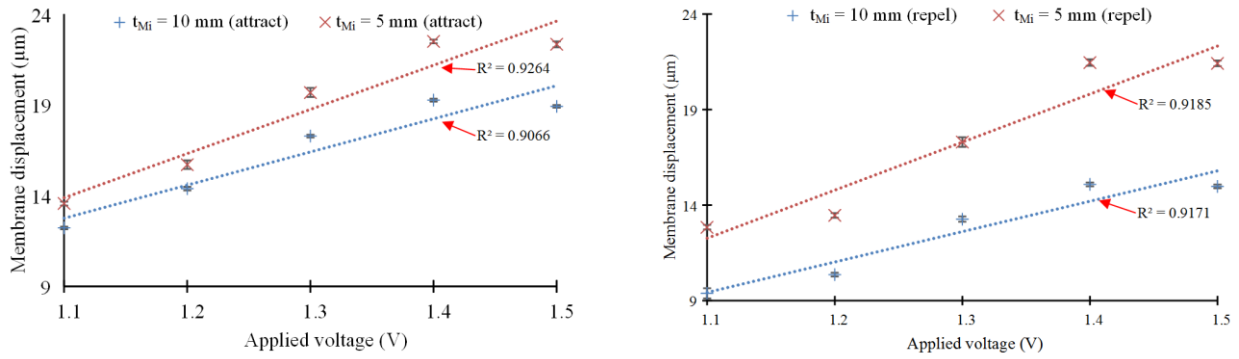

(a) (b)

Fig. 13 Membrane displacement over channel module thickness of 10 mm and 5 mm (a) attraction condition (b) repellant condition

As shown in Fig. 13, as the applied voltage increases, the membrane displacement increases as well. Based on the equation (4), the electromagnetic force is inversely proportional with the length of the gap between the power inductor and permanent magnet. At the maximum permissible voltage supply, 1.4 V, with 5 mm gap, the membrane displacement at attractive and repulsive condition is 22.5 µm and 21.46 µm respectively. Whereas for 10 mm gap configuration, the membrane displacement is reduced to 19.26 µm and 15.08 µm for the attractive and repulsive condition respectively. This is due to the increase of the gap that causes the attraction or repellent force to decrease (based on equation (4), F_e is inversely proportional to t_{Mi}).

5.3 Flow rate experiment with a mechanically driven micropump system

As repulsive and attractive conditions are depending based on the medium in between the power inductor and permanent magnet, this experiment was conducted to investigate the membrane displacement when the microchannel is fully filled with water. The evaluation was studied on the flow rate, Q, performance under a zero backpressure condition. The microchannel chip (body), and the actuation module for this setup were based on our previously reported work [8]. The fabricated membrane sheet from this work was embedded on the top of the microchannel chip to form a single microchannel module device. The applied actuation frequencies from the controller were from 1 – 16 Hz with 1 Hz resolution. Medium for the experiment was water with a density of 1000 kg/m^3. From the experiment, the flow rate is achievable as low as 1 Hz, producing of 0.3045 ± 0.0041 µLs^{-1} (forward direction) and 0.2975 ± 0.0036 µLs^{-1} (reversed direction). The membrane oscillation starts to increase accordingly with the actuation frequency until it reaches to the maximum flow rate, where the membrane vibrates at the optimum value at 9 Hz of the driving frequency, producing of 1.1254 ± 0.0658 µLs^{-1} (forward direction) and 1.1266 ± 0.0760 µLs^{-1} (reversed direction).

6. System benchmark and the potential application

In order to evaluate the device's performance, the micropump was compared in Table 1 with the previously reported mechanically driven micropump system that implements a PDMS membrane sheet as the moving diaphragm. From the reported micropump systems, Ke M.T. *et al.*, provides the highest flow rate of 220 µLs^{-1} with a low operating voltage of 3 V_{dc} [9], but the actuator used was with two ball check valves that easily to eradicate the membrane sheet due to friction. Meanwhile, in a low flow rate application, Junhui *et al.* reported a piezoelectrically actuated micropump with a minimum flow rate of 0.0043 µLs^{-1} by using a pair of flap microvalves [2]. The usage of the active microvalve only creates single direction fluid flow and the flow rate is limited to the opening and closing time of the flap valves. The fatigue of the mechanical moving parts will break the flap and contaminate the working fluid [10]. Meanwhile, in this work, the proposed micropump showed the flow range is in between the larger and small flow rate application; is achievable from 0.2975 µLs^{-1} with 1 Hz of actuation frequency to 1.1266 µLs^{-1} at 9 Hz of optimum actuation frequency with a low operating voltage and power consumption of 1.4 V_{dc} and 48.64 mW respectively.

From the mentioned characteristics, a few applications that were relevant to the developed micropump system were proposed. Micropump is the main part of a drug delivery system that transfers the drug reagents from the drug reservoir to the target place with high performance, accuracy, and reliability [14-16]. To achieve the desired therapeutic effect, the drugs or chemical reagents should be controlled at a certain level of concentration. A number of medical micropumps based on different actuation and pumping mechanisms have been successfully designed such as in blood delivery. Blood is a specialized biological fluid consisting of red blood cells, white cells and platelets suspended in a complex medium known as plasma. Hsu *et al.* reported a biocompatible peristaltic micropump for blood transportation tests [17]. The actuation was based on the piezoelectric actuator, glued onto the membrane sheet. The test blood was injected into the veins of rats to study the biocompatibility of the blood to the trial subject. The typical flow rate required in the delivery operation was 0.8367 µLs^{-1}, which is well suited to the developed micropump system.

Table 1 Performance comparison with other reported electromagnetic driven micropumps

Authors	Microchannel material		Actuation scheme (electromagnet)	Driving method	Q_{max} (µLs^{-1})	Medium
	Body	Membrane				
This work	PDMS	PDMS	Power inductor	Deflection	1.1266	Water
Wonwhi *et al.* 2018 [11]	PDMS	PDMS	Rotating magnet	Deflection	3.75	Water
Kawun *et al.*, 2016 [12]	PDMS	PDMS	Helical coil	Magnet oscillation	2.25	Water
Junhui *et al.*, 2014 [2]	Glass	PDMS	Electroplate film	Deflection	0.0043	Water
Chee *et al.*, 2013 [13]	PDMS	PDMS	Plunger	Pinching	25.33	Water
Ke *et al.*, 2012 [9]	PMMA	PDMS	Microcoil	Deflection	220	Water

7. Conclusion

This chapter shows the development and fabrication of the thin sheet membrane by using a spin coating technique. The flexible diaphragm was fabricated by using a polymer material from SYLGARD® 184 Silicone Elastomer Kit with

a mixing ratio of the resin to hardener 10:1 (w/w). The suitable parameter to fabricate a membrane sheet with a pre-polymer mixture (with a ratio of 10:1) by using a digital spin coater machine were at 2.5 g of PDMS mixture, 500 rpm of spinning speed and 180 s of time taken to yield a 314.82 ± 3.6556 µm thick membrane.

The fabricated membrane was tested by integrating to a microchannel chip where a 4 mm magnet and a power inductor is able to deflect the membrane to a maximum of 22.5 µm in the attractive condition. The gap of the actuation components: magnet and the power inductor show important relation for the membrane displacement trends. As the gap is closer, the membrane deflected more for both attract and repel condition. The medium inside the microchannel between the actuator components also influences the membrane displacement. This fabrication guideline demonstrates the potential of this proposed membrane as a moving diaphragm for a mechanical micropump in various application areas.

Acknowledgments

The authors would like to acknowledge the Ministry of Higher Education of Malaysia for sponsoring this research study through the MyPhD scholarship. This research study was also funded by Research University Grant (Q.J130000.2523.15H88), UTARRF (IPSR/RMC/UTARRF/2017-C1/C01) Vote: 6200/CC8 and FRGS (R.J130000.7823.4F462).

References

[1] M. Shen, C. Yamahata, and M. A. M. Gijs, "Miniaturized PMMA ball-valve micropump with cylindrical electromagnetic actuator," *Microelectronic Engineering*, vol. 85, pp. 1104-1107, May-June 2008.

[2] J. Ni, B. Wang, S. Chang, and Q. Lin, "An integrated planar magnetic micropump," *Microelectronic Engineering*, vol. 117, pp. 35-40, Jan 4 2014.

[3] M.-T. Ke, J.-H. Zhong, and C.-Y. Lee, "Electromagnetically-Actuated Reciprocating Pump for High-Flow-Rate Microfluidic Applications," *Sensors*, vol. 12, pp. 13075-13087, 2012.

[4] M. D. Nguyen, H. Nazeer, M. Dekkers, D. H. A. Blank, and G. Rijnders, "Optimized electrode coverage of membrane actuators based on epitaxial PZT thin films," *Smart Materials and Structures*, vol. 22, p. 085013, 2013.

[5] H. Selvaraj, B. Tan, and K. Venkatakrishnan, "Maskless direct micro-structuring of PDMS by femtosecond laser localized rapid curing," *Journal of Micromechanics and Microengineering*, vol. 21, pp. 075018-075018, 2011.

[6] I. D. Johnston, D. K. McCluskey, C. K. L. Tan, and M. C. Tracey, "Mechanical characterization of bulk Sylgard 184 for microfluidics and microengineering," *Journal of Micromechanics and Microengineering*, vol. 24, p. 035017, 2014.

[7] D. Tsoukalas and C. Tsamis, *Simulation of Semiconductor Processes and Devices 2001: SISPAD 01*: Springer Vienna, 2012.

[8] M. Q. A. Rusli, P. S. Chee, and P. L. Leow, "Characterization of Electromagnetic Valveless Micropump," *TELKOMNIKA (Telecommunication Computing Electronics and Control)*, vol. 15, pp. 771-777, 2016.

[9] M. T. Ke, J. H. Zhong, and C. Y. Lee, "Electromagnetically-Actuated Reciprocating Pump for High-Flow-Rate Microfluidic Applications," *Sensors*, vol. 12, pp. 13075-13087, 2012.

[10] E. Stemme and G. Stemme, "A valveless diffuser/nozzle-based fluid pump," *Sensors and Actuators A: Physical*, vol. 39, pp. 159-167, November 01 1993.

[11] W. Na, J. Kim, H. Lee, B. Yoo, and S. Shin, "Asymmetric fluttering ferromagnetic bar-driven inertial micropump in microfluidics," *Biomicrofluidics*, vol. 12, p. 014115, 2018/01// 2018.

[12] P. Kawun, S. Leahy, and Y. Lai, "A thin PDMS nozzle/diffuser micropump for biomedical applications," *Sensors and Actuators A: Physical*, vol. 249, pp. 149-154, October 1 2016.

[13] P. S. Chee, R. Abdul Rahim, R. Arsat, U. Hashim, and P. L. Leow, "Bidirectional flow micropump based on dynamic rectification," *Sensors and Actuators A: Physical*, vol. 204, pp. 107-113, 2013.

[14] S. T. Sanjay, W. Zhou, M. Dou, H. Tavakoli, L. Ma, F. Xu, *et al.*, "Recent advances of controlled drug delivery using microfluidic platforms," *Advanced Drug Delivery Reviews*, vol. 128, pp. 3-28, 2018/03/15/ 2018.

[15] R. Goffredo, A. Pecora, L. Maiolo, A. Ferrone, E. Guglielmelli, and D. Accoto, "A Swallowable Smart Pill for Local Drug Delivery," *Journal of Microelectromechanical Systems*, vol. 25, pp. 362-370, 2016.

[16] R. Mishra, T. K. Bhattacharyya, and T. K. Maity, "Design and Simulation of Microfluidic Components towards Development of a Controlled Drug Delivery Platform," in *2016 29th International Conference on VLSI Design and 2016 15th International Conference on Embedded Systems (VLSID)*, 2016, pp. 583-584.

[17] Y.-C. Hsu, S.-J. Lin, and C.-C. Hou, "Development of peristaltic antithrombogenic micropumps for in vitro and ex vivo blood transportation tests," *Microsyst. Technol.*, vol. 14, pp. 31-41, 2008.